Unusual valence state and metal-insulator transition in $BaV_{10}O_{15}$ probed by hard x-ray photoemission spectroscopy

T. Yoshino,[1] M. Okawa,[2] T. Kajita,[3] S. Dash,[1] R. Shimoyama,[2] K. Takahashi,[2] Y. Takahashi,[2] R. Takayanagi,[2] T. Saitoh,[2] D. Ootsuki,[4] T. Yoshida,[4] E. Ikenaga,[5] N. L. Saini,[6] T. Katsufuji,[3] and T. Mizokawa[1]

[1]*Department of Applied Physics, Waseda University, Shinjuku, Tokyo 169-8555, Japan*

[2]*Department of Applied Physics, Tokyo University of Science, Katsushika, Tokyo 125-8585, Japan*

[3]*Department of Physics, Waseda University, Shinjuku, Tokyo 169-8555, Japan*

[4]*Graduate School of Human and Environmental Studies, Kyoto University, Sakyo, Kyoto 606-8501, Japan*

[5]*Japan Synchrotron Radiation Research Institute, Sayo, Hyogo 679-5198, Japan*

[6]*Department of Physics, University of Roma "La Sapienza" Piazzale Aldo Moro 2, 00185 Roma, Italy*

(Received 27 December 2016; revised manuscript received 3 February 2017; published 27 February 2017)

We have studied the electronic structure of $BaV_{10}O_{15}$ across the metal-insulator transition with V trimerization by means of hard-x-ray photoemission spectroscopy (HAXPES) and mean-field calculations. The V $2p$ HAXPES indicates $V^{2.5+}$-V^{3+} charge fluctuation in the metallic phase, and V^{2+}-V^{3+} charge order in the insulating phase. The $V^{2.5+}$-V^{3+} charge fluctuation is consistent with the mean-field solution where a V $3d$ a_{1g} electron is shared by two V sites with face-sharing VO_6 octahedra. The valence-band HAXPES of the metallic phase exhibits pseudogap opening at the Fermi level associated with the charge fluctuation, and a band gap ∼200 meV is established in the insulating phase due to the switching of charge correlation.

DOI: 10.1103/PhysRevB.95.075151

I. INTRODUCTION

Metal-insulator transitions (MITs) in transition-metal compounds (TMCs) are generally driven by electron-electron and electron-lattice interactions of the transition-metal d electrons [1,2]. While MITs with Mott localization in integer valence TMCs are governed by an on-site Coulomb interaction between d electrons, MITs with charge ordering in noninteger valence TMCs may have different causes, such as Wigner crystallization by intersite electron-electron interactions, dimerization/trimerization by electron-lattice interactions, and polaronic or Jahn-Teller-type lattice distortions. For example, the electron-lattice interaction is essential to stabilize the stripe-type charge order in perovskite-type $La_{2-x}Sr_xNi^{2+/3+}O_4$, where NiO_6 octahedra share the corners with their neighbors [3–5]. On the other hand, the intersite Coulomb interaction between d electrons plays an essential role for the zigzag-type charge order of $NaV_2{}^{4+/5+}O_5$ where VO_5 pyramids share the corners in the ladder structure [6–8].

The physics of charge orders in TMCs is very rich and depends on their coordination geometry, valence state, and driving forces involved. Among the various charge ordering phenomena in noninteger valence TMCs, the charge order of V^{2+} and V^{3+} is very rare, and a new physics is expected in a $V^{2+/3+}$ TMC. A $V^{2+/3+}$ mixed valence oxide with the composition of $BaV_{10}O_{15}$ was discovered by Liu *et al.* [9–11] and was found to exhibit interesting physical properties, including a structural transition around 120 K [12–14]. Kajita *et al.* have identified the structural transition at 123 K in single crystal $BaV_{10}O_{15}$ that is driven by V trimerization [15] and V $3d$ orbital order [16]. The structural transition is accompanied by a resistivity drop of two orders of magnitude in going from the low to high temperature phases, and the transition may correspond to a MIT, although the resistivity gradually decreases with increasing temperature even in the high temperature phase. The unit cell of $BaV_{10}O_{15}$ consists of four layers, each of which is constructed from "boat" units with five edge-sharing VO_6 octahedra [Fig. 1(a)]. While the VO_6 octahedra in the first and second (third and fourth) layers share the edges, those in the second and third (first and fourth) layers share the faces. Below the transition temperature, the V trimers are formed, as indicated by thick solid lines in the lower panel of Fig. 1(b). The "boat" units are connected by the trimers in the insulating phase.

V trimerization by V $3d$ orbital ordering is known to occur in $LiV^{3+}O_2$ with a V triangular lattice layer where the VO_6 octahedra share the edges with their neighbors [18–20]. However, the V trimerization in $BaV_{10}O_{15}$ is accompanied by enhanced magnetic susceptibility in contrast to the reduced one in $LiV^{3+}O_2$ due to the formation of three singlet bonds in the trimer. Since the average valence of V is +2.8, $BaV_{10}O_{15}$ is expected to show an interesting interplay between $V^{2+/3+}$ charge order and the V trimerization. In particular, Hund coupling plays an important role in the electronic configurations of V^{2+} and V^{3+}, as shown in Fig. 1(c), which may contradict with the singlet bond formation. Although details of the crystal structure of $BaV_{10}O_{15}$ have been reported in the literature, the electronic structure and the valence state of $BaV_{10}O_{15}$ have yet to be studied by spectroscopic methods, except for optical and x-ray absorption spectroscopy [15,16]. In order to clarify the electronic structural change across the MIT and to reveal the relationship between the V trimerization and the rare $V^{2+/3+}$ charge order, we have performed hard x-ray photoemission spectroscopy (HAXPES) of $BaV_{10}O_{15}$. The valence-band spectral change is consistent with the MIT around 120 K. The V $2p$ spectrum is split into two components above and below the MIT temperature, indicating V $3d$ charge fluctuation and charge order, respectively. Based on the proposed charge/orbital model, the relationship between the present system and the classical systems such as $LiVO_2$ and V_2O_3 will be discussed.

II. EXPERIMENT

Single crystals of $BaV_{10}O_{15}$ were grown as reported in the literature [15]. HAXPES measurements were performed at

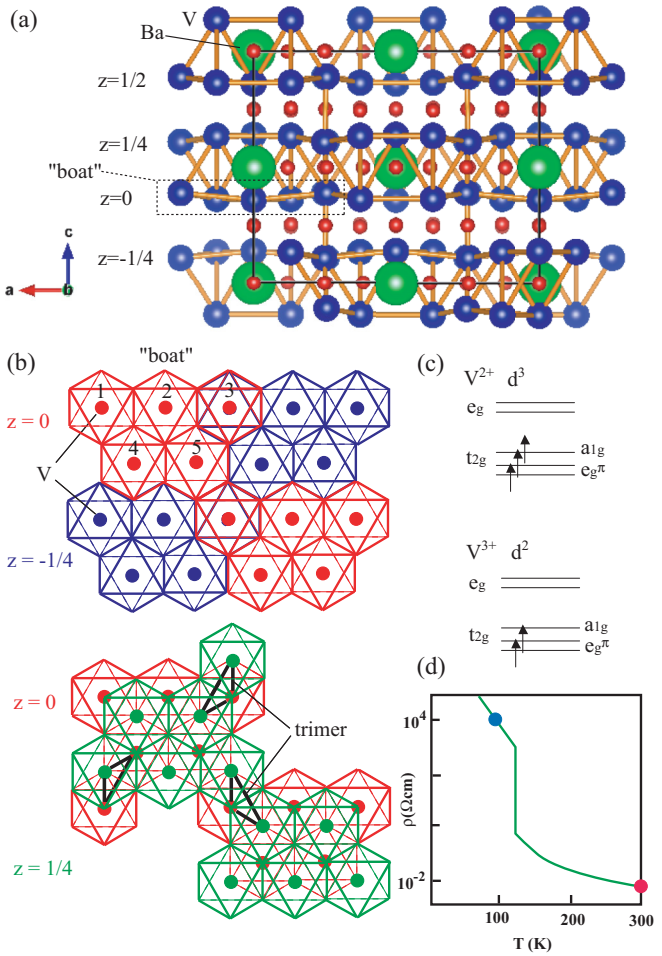

FIG. 1. (a) Crystal structure of $BaV_{10}O_{15}$ at 300 K created by VESTA [17]. The unit cell consists of four layers with $z = 0$, $\frac{1}{4}$, $\frac{2}{4}$, and $-\frac{1}{4}(\frac{3}{4})$. (b) Schematic drawing of the VO_6 octahedra in $BaV_{10}O_{15}$. VO_6 octahedra share the edges in each layer and five octahedra form a boat unit. VO_6 octahedra share the faces between the first ($z = 0$) and fourth ($z = -\frac{1}{4}$) layers and share edges between the first ($z = 0$) and second ($z = \frac{1}{4}$) layers. (c) Electronic configurations of V^{2+} and V^{3+}. The V $3d$ t_{2g} orbitals are split into a_{1g} and two e_g^{π} orbitals under the trigonal ligand field. (d) Schematic drawing of the temperature dependence of resistivity reported by Kajita *et al.* [15]. The circles indicate the temperatures for HAXPES measurements.

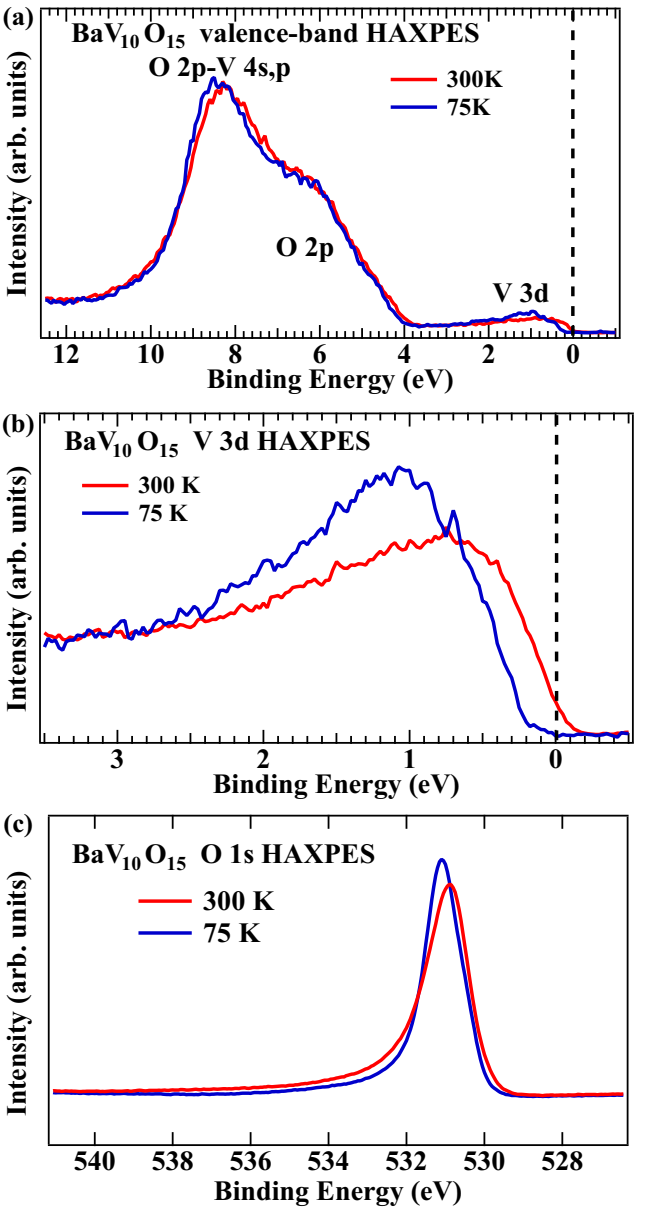

FIG. 2. (a) HAXPES spectra for the entire valence band of $BaV_{10}O_{15}$ taken at 300 and 75 K. (b) HAXPES spectra near the Fermi level of $BaV_{10}O_{15}$ taken at 300 and 75 K. (c) O 1s HAXPES spectra taken at 300 and 75 K.

BL09XU of SPring8 which has the same optics as BL47XU of SPring8 [21]. The crystals were fractured at 300 K under an ultrahigh vacuum of 10^{-6} Pa. The photon energy was set to 7930 eV and the photoelectrons were collected and analyzed by Omicron Scienta R4000-10kV. The pass energy was set to 200 eV and the total energy resolution was about 270 meV. The binding energy was calibrated using the Fermi edge of the Au reference.

III. RESULTS AND DISCUSSION

Figures 2(a) and 2(b) show the valence-band HAXPES spectra across the transition at 123 K. The band gap of ~0.2 eV opens at 75 K in the insulating phase. The magnitude of the band gap is consistent with the optical spectra reported by Kajita *et al.* [15]. At 300 K, the band gap is destroyed and finite spectral weight exists at the Fermi level, indicating that the high temperature phase can be viewed as a metallic state. However, the resistivity gradually decreases with increasing temperature in the high temperature phase and deviates from a simple metallic behavior. Indeed, the spectral weight at the Fermi level is relatively small compared to the intense V $3d$ band around 1 eV below the Fermi level, and a kind of pseudogap remains at the Fermi level. Such an anomalous metallic state with pseudogap behavior has been reported in various transition-metal oxides [1], and, in the present system, it should be related to charge fluctuation observed by V $2p$ HAXPES, which will be discussed later. Here, we speculate that the resistivity gradually decreases with increasing temperature due to a decrease of the charge or orbital fluctuations in the

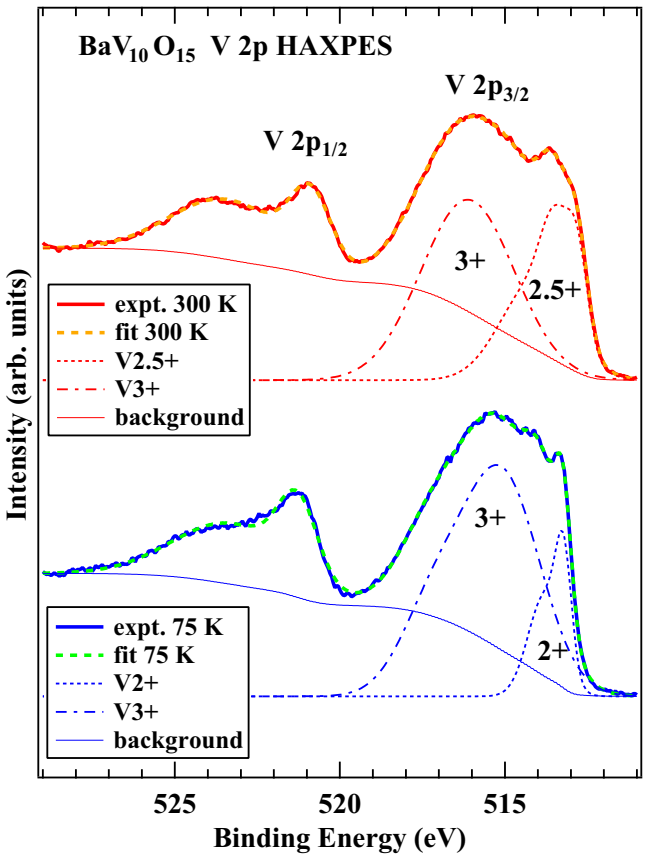

FIG. 3. V $2p$ HAXPES spectra taken at 300 and 75 K. The fitted results are shown by the dashed curves. The low- and high-energy components for V $2p_{3/2}$ are indicated by the dotted and dotted-dashed curves, respectively.

anomalous metallic phase. The line shape of the V $3d$ t_{2g} peak is somewhat similar to that of the Co $3d$ t_{2g} peak of the triangular lattice in Co oxides with a positive and large Seebeck coefficient [22]. However, the Seebeck coefficient is almost zero around room temperature in $BaV_{10}O_{15}$ [13,23], indicating that substantial V $3d$ spectral weight should exist just above the pseudogap and that the electron contribution may be canceled with the hole contribution. The O $1s$ HAXPES of the metallic phase exhibits substantial asymmetry at 300 K due to the screening effect of the V $3d$ conduction electrons.

Figure 3 shows the V $2p$ HAXPES spectra taken at 300 and 75 K (indicated by the thick solid curves). At 300 K, the low binding energy side of the V $2p_{3/2}$ branch reaches 512 eV. In the V $2p$ HAXPES of various metallic V oxides such as $SrVO_3$ [24], VO_2 (metallic phase) [25], and V_2O_3 (metallic phase) [26], the V $2p_{3/2}$ peak was commonly observed to be very broad and extended from ~519 to ~512 eV. The HAXPES studies have established that the broadening of the V $2p_{3/2}$ peak represents the bulk electronic structure and is assigned to the core-hole screening effect by the conducting V $3d$ t_{2g} electrons. It should be recalled that, while metallic systems such as $SrVO_3$ and V_2O_3 have the integer number of the V formal valence, $BaV_{10}O_{15}$ has the noninteger V formal valence. Therefore, in the metallic phase of $BaV_{10}O_{15}$, both the mixed valence effect and the core-hole screening effect should be considered for the interpretation of the V $2p$ spectrum. On the other hand, in the V $2p$ HAXPES taken at 75 K (insulating phase), the V $2p_{3/2}$ peak becomes less broad, which is consistent with the absence of a core-hole screening effect by conducting electrons.

In order to extract quantitative information on the mixed valence, the V $2p$ spectrum of the insulating phase is fitted to six Gaussians (four for $2p_{3/2}$ and two for $2p_{1/2}$) plus a Shirley-type background, as indicated by the dashed curve. First, since the $2p_{1/2}$ main peak overlaps with the charge-transfer satellite for the $2p_{3/2}$ peak in V oxides [27], we focus on the analysis of the $2p_{3/2}$ part. The $2p_{3/2}$ peak would be decomposed into V^{2+} and V^{3+} contributions considering the fact that the average V valence of $BaV_{10}O_{15}$ is +2.8. The $2p_{3/2}$ peak can be decomposed into the low-energy part (with two Gaussians) and the high-energy part (with two Gaussians), which are indicated by dotted and dashed-dotted curves, respectively. The low- and high-energy components (which correspond to V^{2+} and V^{3+} components) are located at ~513 and ~515 eV, consistent with the values reported in the literature [28–30]. The intensity ratio of V^{2+} to V^{3+} is about ~0.2. This value agrees with the ratio expected for the charge order of V^{2+}:V^{3+} = 1:4.

In the next step, the V $2p$ spectrum of the metallic phase is fitted to six Gaussians (four for $2p_{3/2}$ and two for $2p_{1/2}$) plus a Shirley-type background, as indicated by the dashed curve. In the $2p_{3/2}$ branch, three Gaussians are required to fit the complicated line shape of the low-energy part, which is probably due to the screening effect by conducting electrons. On the other hand, a broad Gaussian is enough for the high-energy part. In the present fit result, the intensity ratio of the low-energy component to the high-energy one is ~0.6, which is much larger than the expected value of 0.2. Although the complicated line shape of the low-energy part brings ambiguity to the estimation of the intensity ratio, one can safely conclude that the ratio is closer to 0.6 rather than 0.2. Since the high-energy component should correspond to a valence higher than +2.8, it is reasonable to assign it to V^{3+}. Considering an average valence of +2.8 and an intensity ratio of 0.6, the V valence for the low-energy component is estimated to be $V^{2.5+}$ (namely, $V^{2.5+}$:V^{3+} = 2:3). As mentioned above, the low-energy part assigned to $V^{2.5+}$ exhibits a complicated line shape unlike the high-energy V^{3+} peak given by a simple Gaussian. This indicates that the V $3d$ electrons in the $V^{2.5+}$ part mainly contribute to the conductivity and to the core-hole screening. On the other hand, the V $3d$ electrons in the V^{3+} part are essentially localized even in the metallic phase. Here, we speculate that sites 1 and 3 of the boat unit [see Fig. 1(b)] with face-sharing VO_6 neighbors are $V^{2.5+}$ and that sites 2, 4, and 5 are V^{3+}. Such a charge pattern is indeed supported by mean-field calculations on a multiband Hubbard model, as will be discussed later.

The fit results indicate that the charge order with V^{2+}:V^{3+} = 1:4 in the insulating phase is switched to the charge fluctuation with $V^{2.5+}$:V^{3+} = 2:3 in the metallic phase. As for the charge order state with V^{2+}:V^{3+} = 1:4, one of the five V sites is expected to be V^{2+} in the boat unit. When site 2 of the boat unit is V^{2+} [see Fig. 1(b)], the V trimers are formed by V^{3+}, just as $LiVO_2$. Such a V trimer with V^{3+} is expected to be $S = 0$ in total and the magnetic susceptibility

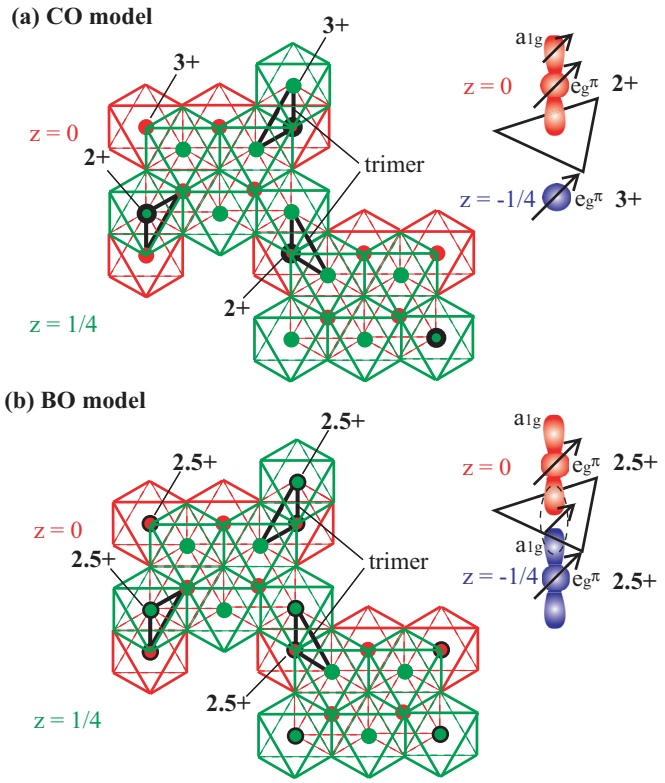

FIG. 4. (a) Charge order of $BaV_{10}O_{15}$ in the insulating phase suggested from the V $2p$ HAXPES and model mean-field calculation. The right panel illustrates the V^{2+} and V^{3+} sites at the face-sharing V-V bond. The V $3d$ a_{1g} orbital is occupied by an electron at the V^{2+} site. (b) Charge fluctuation of $BaV_{10}O_{15}$ in the metallic phase suggested from the V $2p$ HAXPES and model mean-field calculation. The right panel illustrates the $V^{2.5+}$ sites at the face-sharing V-V bond. The V $3d$ a_{1g} orbitals form a molecular orbital to accommodate an electron.

should be reduced below the transition temperature. If site 3 of the boat unit is V^{2+}, as illustrated in Fig. 4(a), one of the trimerized sites should be V^{2+} and the V^{2+}-V^{3+} arrangement is realized in the V-V bond along the c axis (the face-sharing VO_6 octahedra). As illustrated in Fig. 4(a), the a_{1g} and e_g^π orbitals are all occupied at the V^{2+} site with $S = \frac{3}{2}$ while only e_g^π orbitals can be occupied at the V^{3+} site with $S = 1$. Such an orbital configuration favors ferromagnetic coupling between the V^{2+} and V^{3+} sites due to the transfer of the a_{1g} electron and the intra-atomic Hund coupling between the a_{1g} and e_g^π electrons. The transfer of the a_{1g} electron from the V^{2+} to V^{3+} sites is expected to be the lowest-energy charge excitation. This picture is consistent with the smaller optical gap along the c axis than those along the a or b axis [15]. The ferromagnetic interaction due to the a_{1g} electron can be viewed as a Zener double exchange interaction [31]. Also, the ferromagnetic bond mediated by the a_{1g} electron transfer is somewhat similar to the $a_{1g}e_g^\pi$-$e_g^\pi e_g^\pi$ orbital state in the face-sharing V-V bond of V_2O_3 where the V spins are ferromagnetically coupled [32]. In the above charge order model (CO model), one V^{2+} and two V^{3+} form the trimer and a kind of Zener double exchange interaction provides a ferromagnetic coupling between the V^{2+} and V^{3+} sites. This picture is consistent with the enhancement of magnetic susceptibility below the MIT. The V^{2+}-V^{3+} bond with ferromagnetic coupling favors the shorter bond, which is consistent with structural distortion in the insulating phase [15]. On the other hand, the magnetic interaction between the two neighboring trimers is expected to be antiferromagnetic.

In the metallic phase, the V^{2+}-V^{3+} charge order at the face-sharing V-V bond is suppressed, and the $V^{2.5+}$-$V^{2.5+}$ bond would be realized as illustrated in Fig. 4(b). In the bond order model (BO model), the V $3d$ a_{1g} orbitals form a molecular orbital spanning the two V sites to accommodate an electron whereas the e_g^π electrons are localized at each V site. In the fit results for the V $2p$ HAXPES, the $V^{2.5+}$ component is very broad and the binding energy is smaller than the V^{2+} peak in the insulating phase. Most probably, the broad $V^{2.5+}$ peak is derived from the screening effect of the a_{1g} electron shared by the two V sites. When a V $2p$ core hole is created in one of the two V sites, the a_{1g} electron shared by the two sites is transferred to the core-hole site and the well screened structure appears as the lowest-energy part of the V $2p$ HAXPES.

The BO state is indeed obtained in the mean-field calculations on the V $3d$-O $2p$ multiband Hubbard model which were originally proposed to describe orbital order [33] and charge order [34] in perovskite-type transition-metal oxides. The mean-field calculations on the multiband Hubbard model have been applied to possible charge ordered states in $Li_x CoO_2$ with edge-sharing CoO_6 octahedra [35]. In the V $3d$-O $2p$ multiband Hubbard Hamiltonian for $BaV_{10}O_{15}$, the V $3d$-V $3d$ Coulomb interactions and the O $2p$-V $3d$, O $2p$-O $2p$, and V $3d$-V $3d$ transfer integrals are described by Kanamori and Slater-Koster parameters, respectively. A typical parameter set for Kanamori parameters for V oxides is $u = 6.1$ eV, $u' = 4.66$ eV, $j = 0.72$ eV, and that for Slater-Koster parameters is $(pd\sigma) = -1.8$ eV, $(pd\pi) = 0.81$ eV, $(pp\sigma) = 0.6$ eV, $(pp\pi) = -0.15$ eV, $(dd\sigma) = -0.3$ eV, and $(dd\pi) = 0.15$ eV [33]. The bare V $3d$ energy level relative to O $2p$ ($\epsilon_d - \epsilon_p$) is set to -3.0 eV, namely, the O $2p$ to V $3d$ charge-transfer energy ($\epsilon_d - \epsilon_p + 2U$, $U = u - 20j/9$) is set to 6.0 eV, which is a typical value for V^{3+} oxides [33]. The mean-field treatment is applied to the V $3d$-V $3d$ Coulomb interactions. Starting from initial values of the order parameters (including the occupation numbers of the V $3d$ orbitals), diagonalization of the mean-field Hamiltonian and calculations of the order parameters are iterated until successive differences of all the order parameters converge to less than 10^{-4}. The BO state is obtained as one of the stable mean-field solutions of the V $3d$-O $2p$ multiband Hubbard Hamiltonian for $BaV_{10}O_{15}$. The BO state is robust even when the parameter values in the Hamiltonian except j are moderately changed. It has been found that the Hund exchange j close to the atomic value is essential to stabilize the BO state. In the calculation with the parameter set, the BO state with the V $3d$ a_{1g} electron in the face-sharing V-V bond is lower in energy than an antiferromagnetic and CO state with V^{2+} at site 2 and V^{3+} at sites 1, 3, 4, and 5 of the boat. The energy difference of the two states is ~0.5 eV per formula unit and ~0.05 eV per V site. On the other hand, the CO state of Fig. 4(b) (V^{2+} at site 3) cannot be stabilized relative to the BO state without lattice distortions. V-V bond shortening, which is consistent

with the trimerization, is required to stabilize the CO state with V^{2+} at site 3 against the BO state.

IV. CONCLUSION

In conclusion, the electronic structure of the unique MIT system $BaV_{10}O_{15}$ has been revealed by means of hard-x-ray photoemission spectroscopy. On the basis of V $2p$ HAXPES results, the $V^{2.5+}$-V^{3+} charge fluctuation is suggested in the metallic phase. On the other hand, V^{2+}-V^{3+} charge order with V^{2+}:V^{3+} = 1:4 is established in the insulating phase. The valence-band HAXPES shows a pseudogap opening at the Fermi level in the metallic phase which is associated with the charge fluctuation. The $V^{2.5+}$-$V^{2.5+}$ state in the face-sharing V sites is stabilized by the molecular orbital formation of the V $3d$ a_{1g} orbital. In order to explain the results of the V $2p$ HAXPES experiment and model mean-field calculations, the V^{2+}-V^{3+} charge order should develop in the face-sharing V sites under electron-lattice coupling. The a_{1g} electron in the V^{2+} site can induce ferromagnetic coupling of the V^{2+}-V^{3+} bonds within the V trimer due to the Zener double exchange. The physics of V trimerization in $BaV_{10}O_{15}$ is different from that of $LiVO_2$, and the importance of the a_{1g} orbital in the face-sharing V sites is rather similar to that in V_2O_3. The ferromagnetic V trimer in $BaV_{10}O_{15}$ as indicated by the present study would be related to the trimer observed in ferrimagnetic Fe_3O_4 [36].

ACKNOWLEDGMENTS

The authors would like to thank Professor L. H. Tjeng and Professor G. A. Sawatzky for enlightening discussions. This work was supported by CREST-JST and Grant-in-Aids for Scientific Research from JSPS (No. 26400321 and No. 16H04020). The synchrotron radiation experiment was performed with the approval of SPring-8 (2016B1005).

[1] M. Imada, Y. Tokura, and A. Fujimori, Rev. Mod. Phys. **70**, 1039 (1998).
[2] D. I. Khomskii, *Transition Metal Compounds* (Cambridge University Press, Cambridge, UK, 2014).
[3] S. Anissimova, D. Parshall, G. D. Gu, K. Marty, M. D. Lumsden, Songxue Chi, J. A. Fernandez-Baca, D. L. Abernathy, D. Lamago, J. M. Tranquada, and D. Reznik, Nat. Commun. **5**, 3467 (2014).
[4] J. Zaanen and P. B. Littlewood, Phys. Rev. B **50**, 7222 (1994).
[5] K. Rościszewski and A. M. Oleś, J. Phys.: Condens. Matter **23**, 265601 (2011).
[6] H. Sawa, E. Ninomiya, T. Ohama, H. Nakao, K. Ohwada, Y. Murakami, Y. Fujii, Y. Noda, M. Isobe, and Y. Ueda, J. Phys. Soc. Jpn. **71**, 385 (2002).
[7] H. Seo and H. Fukuyama, J. Phys. Soc. Jpn. **67**, 2602 (1998).
[8] M. V. Mostovoy and D. I. Khomskii, Solid State Commun. **113**, 159 (1999).
[9] D. Chales de Beaulieu and H. Müller-Buschbaum, Z. Naturforsch. B **35**, 669 (1980).
[10] E. Cuno and H. Muüller-Buschbaum, Z. Anorg. Allg. Chem. **572**, 89 (1989).
[11] G. Liu and J. E. Greedan, J. Solid State Chem. **110**, 274 (1994).
[12] G. Liu and J. E. Greedan, J. Solid State Chem. **122**, 416 (1996).
[13] C. A. Bridges and J. E. Greedan, J. Solid State Chem. **177**, 1098 (2004).
[14] C. A. Bridges, T. Hansen, A. S. Wills, G. M. Luke, and J. E. Greedan, Phys. Rev. B **74**, 024426 (2006).
[15] T. Kajita, T. Kanzaki, T. Suzuki, J. E. Kim, K. Kato, M. Takata, and T. Katsufuji, Phys. Rev. B **81**, 060405(R) (2010).
[16] K. Takubo, T. Kanzaki, Y. Yamasaki, H. Nakao, Y. Murakami, T. Oguchi, and T. Katsufuji, Phys. Rev. B **86**, 085141 (2012).
[17] K. Momma and F. Izumi, J. Appl. Crystallogr. **44**, 1272 (2011).
[18] J. Kikuchi, S. Kambe, H. Yasuoka, Y. Ueda, K. Tomimoto, and J. Akimitsu, J. Phys. Soc. Jpn. **60**, 3620 (1991).
[19] H. F. Pen, J. van den Brink, D. I. Khomskii, and G. A. Sawatzky, Phys. Rev. Lett. **78**, 1323 (1997).
[20] T. Jin-no, Y. Shimizu, M. Itoh, S. Niitaka, and H. Takagi, Phys. Rev. B **87**, 075135 (2013).
[21] E. Ikenaga, M. Kobata, H. Matsuda, T. Sugiyama, H. Daimon, and K. Kobayashi, J. Electron Spectrosc. Relat. Phenom. **190**, 180 (2013).
[22] T. Mizokawa, L. H. Tjeng, P. G. Steeneken, N. B. Brookes, I. Tsukada, T. Yamamoto, and K. Uchinokura, Phys. Rev. B **64**, 115104 (2001).
[23] T. Katsufuji, T. Okuda, R. Murata, T. Kanzaki, K. Takayama, and T. Kajita, J. Phys. Soc. Jpn. **85**, 013703 (2016).
[24] J. Laverock, J. Kuyyalil, B. Chen, R. P. Singh, B. Karlin, J. C. Woicik, G. Balakrishnan, and K. E. Smith, Phys. Rev. B **91**, 165123 (2015).
[25] S. Suga, A. Sekiyama, S. Imada, T. Miyamachi, H. Fujiwara, A. Yamasaki, K. Yoshimura, K. Okada, M. Yabashi, K. Tamasaku, A. Higashiya, and T. Ishikawa, New J. Phys. **11**, 103015 (2009).
[26] G. Panaccione, M. Sacchi, P. Torelli, F. Offi, G. Cautero, R. Sergo, A. Fondacaro, C. Henriquet, S. Huotari, G. Monaco, and L. Paolasini, J. Electron Spectrosc. Relat. Phenom. **156–158**, 64 (2007).
[27] A. E. Bocquet, T. Mizokawa, K. Morikawa, A. Fujimori, S. R. Barman, K. Maiti, D. D. Sarma, Y. Tokura, and M. Onoda, Phys. Rev. B **53**, 1161 (1996).
[28] P. H. Citrin, P. Eisenberger, and D. R. Hamann, Phys. Rev. Lett. **33**, 965 (1974).
[29] G. A. Sawatzky and D. Post, Phys. Rev. B **20**, 1546 (1979).
[30] M. C. Biesinger, L. W. M. Lau, A. R. Gerson, and R. St. C. Smart, Appl. Surf. Sci. **257**, 887 (2010).
[31] D. V. Efremov, J. van den Brink, and D. I. Khomskii, Nat. Mater. **3**, 853 (2004).
[32] J.-H. Park, L. H. Tjeng, A. Tanaka, J. W. Allen, C. T. Chen, P. Metcalf, J. M. Honig, F. M. F. de Groot, and G. A. Sawatzky, Phys. Rev. B **61**, 11506 (2000).
[33] T. Mizokawa and A. Fujimori, Phys. Rev. B **54**, 5368 (1996).
[34] T. Mizokawa and A. Fujimori, Phys. Rev. B **56**, 11920 (1997).
[35] T. Mizokawa, Y. Wakisaka, T. Sudayama, C. Iwai, K. Miyoshi, J. Takeuchi, H. Wadati, D. G. Hawthorn, T. Z. Regier, and G. A. Sawatzky, Phys. Rev. Lett. **111**, 056404 (2013).
[36] M. S. Senn, J. P. Wright, and J. P. Attfield, Nature (London) **481**, 173 (2012).